In situ liquid-cell electron microscopy of colloid aggregation and growth dynamics

Joseph M. Grogan,[1,*] Lolita Rotkina,[2] and Haim H. Bau[1,†]

[1]*Department of Mechanical Engineering and Applied Mechanics, University of Pennsylvania, 220 South 33rd Street, Philadelphia, Pennsylvania 19104, USA*

[2]*Penn Regional Nanotechnology Facility, University of Pennsylvania, 3231 Walnut Street, Philadelphia, Pennsylvania 19104, USA*

(Received 26 October 2010; revised manuscript received 21 February 2011; published 16 June 2011)

We report on real-time observations of the aggregation of gold nanoparticles using a custom-made liquid cell that allows for *in situ* electron microscopy. Process kinetics and fractal dimension of the aggregates are consistent with three-dimensional cluster-cluster diffusion-limited aggregation, even for large aggregates, for which confinement effects are expected. This apparent paradox was resolved through *in situ* observations of the interactions between individual particles as well as clusters at various stages of the aggregation process that yielded the large aggregates. The liquid cell described herein facilitates real-time observations of various processes in liquid media with the high resolution of the electron microscope.

DOI: 10.1103/PhysRevE.83.061405 PACS number(s): 83.80.Hj, 47.57.−s, 47.61.−k, 61.46.−w

I. INTRODUCTION

Since its inception in the 1930s, the transmission electron microscope (TEM) has provided a powerful means to image features with nanometer resolution. TEM imaging is performed in a high vacuum chamber and requires very thin slices of the imaged sample. Until recently, TEM imaging has been limited to solid and/or "frozen" samples. To study a process occurring in liquid media, one must typically freeze samples at various stages of the process and carry out *ex situ* imaging. Although this procedure has resulted in major advances in disciplines ranging from materials science to biology, it suffers from some limitations. Imaging of frozen samples does not capture the dynamics of a process, only static snapshots along the way. Moreover, it is difficult to select the "right" moment at which to freeze the sample, so critical observations may be precluded. Also, the essential sample preparation process may alter the sample in fundamental ways. Liquid-cell *in situ* TEM is a burgeoning technique that makes it possible to view processes taking place in liquid media with an electron microscope and has the potential to produce new insights in many branches of science.

The past few years have seen a flare of efforts to develop devices that allow real-time, *in situ* imaging of dynamical, nanoscale processes in fluids with the resolution of a TEM or STEM (scanning TEM) [1–12]. Liquid-cell TEM-STEM devices confine a thin slice of liquid sample in a sealed chamber sandwiched between two electron-transparent membranes, thus preventing evaporation while allowing the electron beam to pass through the sample to produce an image. The liquid slice must be sufficiently thin to minimize electron scattering by the suspending medium, so researchers have relied on microfabrication technology to produce a variety of devices based on a common theme: thin membranes separated by a spacer material to form a sealed chamber. The details of each device differ in the choice of membrane material, sealing method, and spacer material, which dictates the distance between the membranes and the height of the liquid cell. Recently, Zheng *et al*. studied nanoparticle migration in a liquid-cell TEM device and reported on anomalous diffusion behavior [2]. In their experiment, the observed phenomena may have been influenced by leakage from the liquid cell.

We report on real-time electron microscope imaging of colloid aggregation, facilitated by a nanofluidic liquid-cell TEM device, the nanoaquarium (Fig. 1). In contrast to Zheng *et al*.'s device, the nanoaquarium is perfectly sealed. The deduced kinetics of the observed phenomenon in the early stages of aggregate growth agreed well with predictions based on three-dimensional cluster-cluster diffusion-limited aggregation models. Interestingly, large aggregates exhibited properties of clusters grown in a three-dimensional regime, even when the characteristic size of the clusters exceeded the height of the nanoaquarium (tens of nanometers) and two-dimensional growth characteristics may have been expected. The mechanism for this seemingly paradoxical result was revealed through direct observation of the aggregation process, facilitated by the nanoaquarium.

II. METHOD

We investigated diffusion-limited aggregation of gold colloids in water using the nanoaquarium. The nanoaquarium is made by direct bonding of silicon wafers coated with silicon nitride. One of the wafers also contains a thin film of patterned silicon oxide that defines the geometry and height of the chamber and conduits. The thickness of the silicon oxide film, and thus the liquid-cell's height, is controllable and can be prescribed to be tens to hundreds of nanometers. The fabrication steps of the liquid cell have been described previously [1]. The device featured in Fig. 1 has a silicon oxide film that is 100 nm thick, and the imaging window is made of two 50-nm-thick silicon nitride membranes. The device fits into a custom-made holder and can sustain the high vacuum environment of the electron microscope for many hours without any noticeable loss of liquid. Some of the nanoaquarium's highlights include an exceptionally thin sample cross section, wafer scale processing that enables high-yield mass production, robust hermetic sealing that provides leak-free operation, compatibility with lab-on-chip

*jgrogan@seas.upenn.edu
†bau@seas.upenn.edu

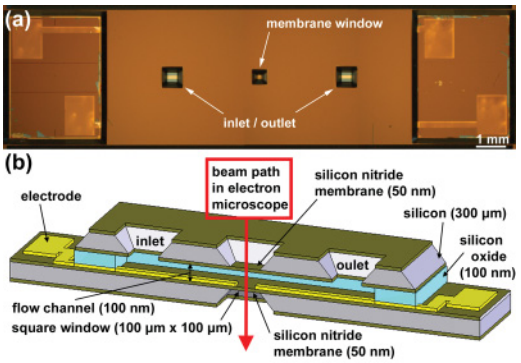

FIG. 1. (Color online) The nanoaquarium. (a) Top-view photograph featuring the silicon nitride observation window and inlet and outlet ports. (b) A schematic of the cross section.

technology, and on-chip integrated electrodes for sensing and actuation.

Aggregation is a classical topic of broad interest in disciplines such as condensed matter physics, material science, air and water pollution, and medicine. Nanoparticle aggregation is of interest, among other things, for the synthesis of colloidal crystals and the formation of meta and ceramic materials with unique properties. Some of the earliest experimental work in the field of nanoscale colloid aggregation and growth was performed by Weitz *et al.* [13,14] and Lin *et al.* [15,16] on systems of aqueous gold colloids undergoing irreversible kinetic aggregation to form tenuous, chainlike fractal structures. Since then, a rich theoretical and modeling framework has been developed with emphasis on kinetic models [17–19] and computer simulations with applications of the Smoluchowsky theory [20–24]. To this day, however, experimental work that captures the dynamics of nanoscale colloid assembly or crystallization is scarce [25], due in large part to the difficulty of *in situ* observation of complicated nanoscale phenomena in liquid media with an appropriate level of spatial and temporal resolution. A common experimental approach is to grow aggregates or crystals under prescribed conditions (e.g., by hydrothermal coarsening) and then freeze the sample to examine the resultant structure with TEM to indirectly infer details of the growth mechanism [26–29]. Except for some unique cases [26,30], this technique does not capture the dynamics of the aggregation process. Dynamic light scattering and static light scattering are common experimental techniques for studying particles in solution. While these techniques provide dynamical information regarding aggregate size and fractal dimension, they are ensemble techniques that give bulk statistics averaged over the cluster mass distribution [16] and cannot capture individual events. In contrast, with the nanoaquarium, one can collect statistical information on an ensemble of clusters in view while also observing interactions between individual particles and clusters.

III. EXPERIMENT

In our experiments, an aqueous solution of amorphous, charge-stabilized, 5-nm-diam gold colloids (EM.GC5, BBI Life Sciences) was drawn into the nanoaquarium by surface tension forces. Imaging was carried out with a FEI Quanta 600 FEG Mark II with a STEM detector. The microscope was operated at 20–30 kV. Better resolution would likely be attained with higher power TEM's (acceleration voltage of up to 300 kV). The nanoaquarium was translated within the microscope to observe various regions of the imaging window. Some of the regions featured small clusters of particles in the process of aggregating (Fig. 2) and others contained sizable aggregates (Fig. 3). See supplemental material for a video of the process that led to Fig. 2 [31].

IV. MODEL

A simple kinetic model that characterizes the aggregation process was proposed by Meakin [32]. Briefly, the number of clusters (N) is inversely proportional to the mean cluster size (S) measured by the number of primary particles composing the cluster:

$$N \sim S^{-1}. \tag{1}$$

The mean cluster radius (R) measured by a bounding circle is

$$R \sim S^{1/D_f}, \tag{2}$$

where D_f is the fractal dimension of the clusters. A coarse-grain model describes the rate of decrease in the number of clusters:

$$\frac{dN}{dt} \sim -(N)(NR^d)(R^2/S^\gamma)^{-1}. \tag{3}$$

The term in the second set of parentheses on the right-hand side of Eq. (3) represents the probability that a cluster will encounter another cluster. The exponent d (=3) is the space

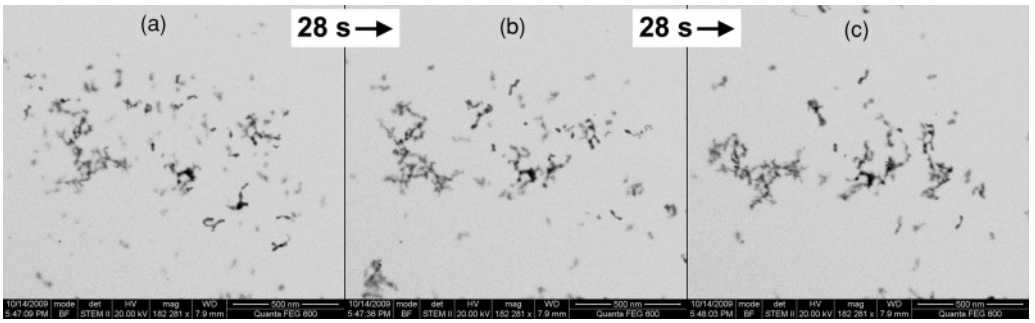

FIG. 2. Aggregating nanoparticles. Three frames from recorded video of 5-nm gold particles and clusters composed thereof, as observed *in situ* with STEM.

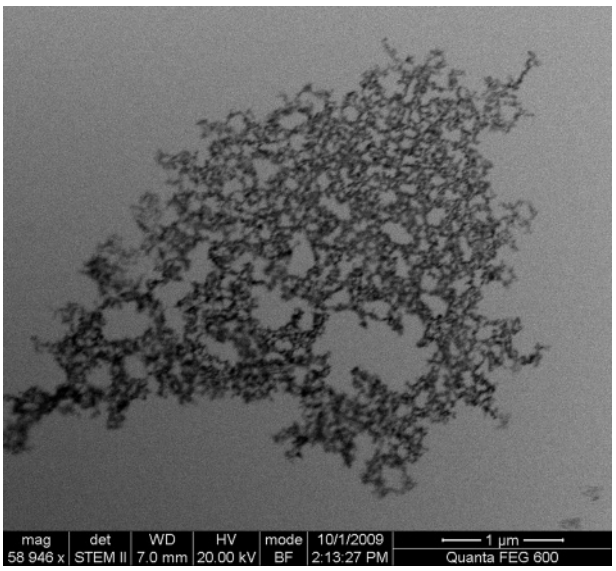

FIG. 3. An aggregate composed of 5-nm-diam gold particles. The fractal dimension, $D_f \sim 1.77$, is consistent with three-dimensional cluster-cluster diffusion-limited aggregation.

dimension. The third term represents the inverse of the average time interval between collisions. The diffusion coefficient of a cluster containing S particles is

$$D \sim S^{\gamma}. \tag{4}$$

Substituting Eqs. (1) and (2) into Eq. (3) yields

$$\frac{dN}{dt} \sim -N^{v}, \tag{5}$$

where

$$v = 2 + 2/D_f - d/D_f - \gamma. \tag{6}$$

Integrating Eq. (5), we have

$$N \sim (t + t_0 + 1)^{1/(1-v)}. \tag{7}$$

In the above, $t = 0$ is the time when observations began, and $t = -t_0$ is the start of the aggregation process. According to the Stokes-Einstein equation, the diffusion coefficient is

$$D = \frac{k_B T}{6\pi\mu R} = \frac{k_B T}{6\pi\mu S^{1/D_f}}, \tag{8}$$

where μ is the viscosity of the suspending medium, k_B is the Boltzmann constant, and T is the temperature. With the aid of Eq. (4), we conclude that the exponent

$$\gamma = -1/D_f. \tag{9}$$

Substituting Eq. (9) into Eq. (6) with $d = 3$ results in $v = 2$. Thus,

$$N \sim (t + t_0 + 1)^{-1}, \tag{10}$$

$$S \sim (t + t_0 + 1), \tag{11}$$

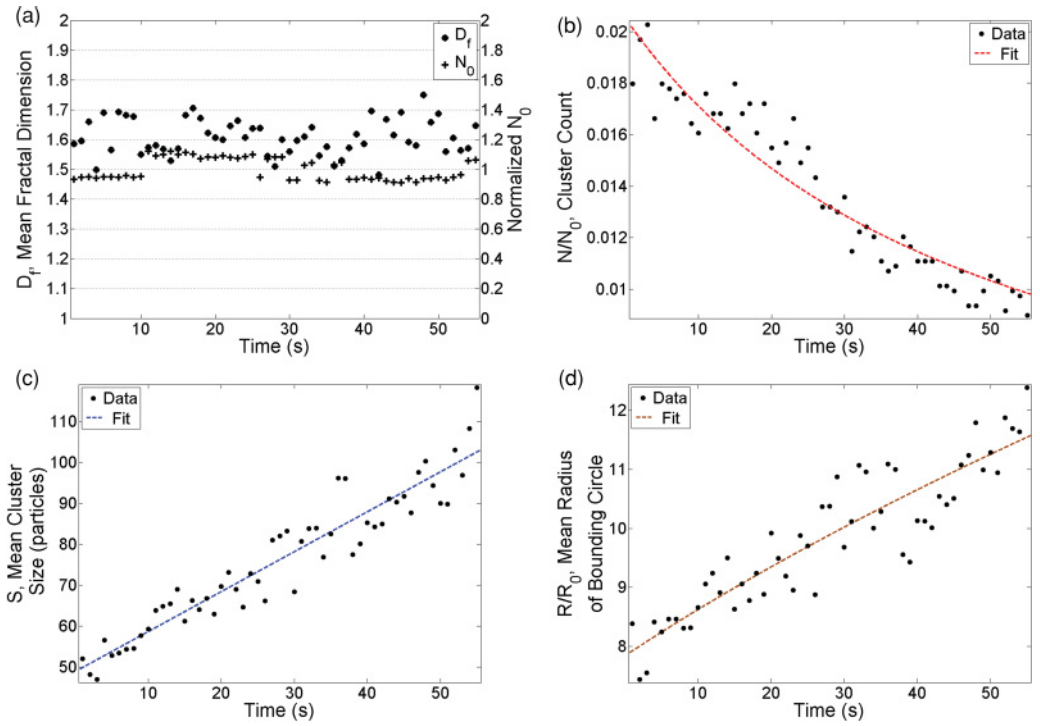

FIG. 4. (Color online) Analysis of the diffusion-limited aggregation process pictured in Fig. 2. The symbols and lines correspond, respectively, to raw data and least-squares fits. (a) The mean fractal dimension (D_f) trends upward as a function of time as the aggregates acquire individual particles and small clusters. The number of primary particles (N_0) accounted for in the image, normalized by the time average of N_0, varies by <20% and indicates that mass is conserved. (b) The number of clusters decays as $(t + 1)^{-1}$. (c) The mean cluster size increases nearly linearly with time. (d) The mean cluster radius grows with an exponent of $1/D_f = 0.5$. The scatter of the data can be attributed, in part, to particles and clusters moving in and out of the field of view from one frame to the next.

and

$$R \sim (t + t_0 + 1)^{1/D_f}. \quad (12)$$

V. ANALYSIS

The video footage for the process pictured in Fig. 2 was analyzed using ImageJ, and nonlinear least-squares fitting of the data was performed with Matlab. Figure 4 depicts D_f (mean for all clusters in view) and N_0, the number of primary particles present in the image (whether alone or as part of a cluster) (a); N (b); S (c); and R (d) as functions of time for a single set of analyzed images (see supplementary material for further details of the image processing and image analysis, as well as details of the subsequent data fitting [31]). As time progresses, D_f increases slowly toward its asymptotic, long-term value of $D_f \sim 1.77$ (measured for Fig. 3), which is in good agreement with Meakin's computational results for cluster-cluster aggregation ($D_f \sim 1.75$–1.80) [32] and Weitz *et al.*'s experimental results for diffusion-limited aggregation of gold nanoparticles ($D_f \sim 1.75$) [13]. The fitted exponent for N is -1.0 ± 0.1 and the fitted exponent for S is 1.0 ± 0.1, in close agreement with theory. The fitted exponent for R is 0.5 ± 0.2, which is approximately the inverse of the time-averaged fractal dimension [Fig. 4(a)]: $(\langle D_f \rangle)^{-1} \sim 0.62$. The good agreement between theory and experiments indicates that the Stokes-Einstein equation adequately describes the diffusion of nanoparticles in the nanosized fluid cell. This is in contrast to the results of Zheng *et al.* [2], whose liquid cell was subject to leakage and associated effects that could include evaporation, convective flow, capillary forces, and nucleation of vapor bubbles.

Interestingly, the lateral dimension of the cluster pictured in Fig. 3 is an order of magnitude larger than the cluster's height (dictated by the nanochannel's height); yet the fractal dimension is consistent with three-dimensional growth, rather than two-dimensional growth. Theoretical models for simple diffusion-limited aggregation, in which particles are added one at a time to a single immobile growing cluster via random-walk trajectories, predict clusters with $D_f \sim 1.72$ for two-dimensional growth and $D_f \sim 2.5$ for three-dimensional growth [32]. These models are, however, inappropriate for our experiments. In our experiments, clusters are not immobilized; they clearly move and combine (see Fig. 2 and supplemental material video [31]). Even the largest clusters, such as the one in Fig. 3, were mobile during most of the experiment. Theoretical models for cluster-cluster diffusion-limited aggregation, in which particles and clusters are allowed to move via random-walk trajectories and combine, predict clusters with $D_f \sim 1.4$–1.45 for two-dimensional growth and $D_f \sim 1.75$–1.8 for three-dimensional growth [32]. This raises the following question: why do relatively large clusters exhibit characteristics of three-dimensional growth while two-dimensional growth might have been expected?

Our *in situ* imaging helps to shed light on the formation of large aggregates in a shallow conduit. Initially, clusters assemble from individual particles that are small relative to the conduit height, and follow a three-dimensional growth habit, as illustrated in Fig. 4. Subsequently, when the size of the clusters approaches the height of the channel, the clusters' movement is confined to a plane and growth is dominated by lateral cluster-cluster aggregation. Since these aggregating clusters already possess characteristics of growth in a near-three-dimensional regime, these characteristics are preserved in the resulting aggregate. Figure 5 depicts two clusters with fractal dimensions of ~1.67 and ~1.65 [appropriate values considering the upward trend of D_f in Fig. 4(a)] coming together to form a larger cluster with a fractal dimension of ~1.64. Additionally, small clusters and individual particles are free to diffuse into the body of a large cluster, further adding to the structural complexity of the aggregate. Figure 6 depicts the fractal dimension as a function of aggregate size for several aggregates observed in our experiments. As the cluster size increases, there is a narrowing of the variation in fractal dimension, along with an upward trend in the fractal dimension toward the long-term value consistent with three-dimensional growth.

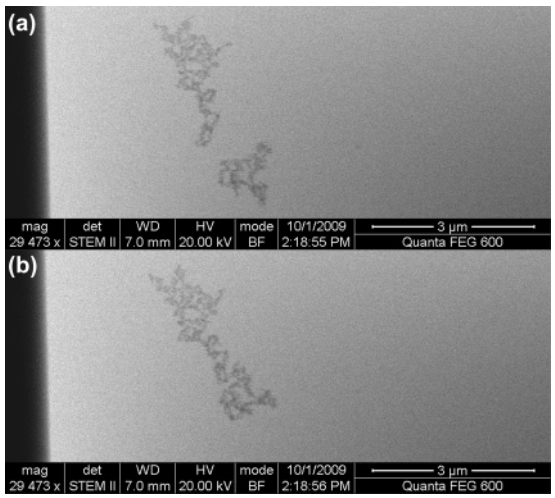

FIG. 5. Cluster-cluster aggregation. Two distinct clusters (a) come together to form a single cluster one second later (b). Small clusters formed in a three-dimensional growth regime go on to aggregate two-dimensionally, resulting in large aggregates with three-dimensional characteristics, despite confinement in a narrow channel.

FIG. 6. Fractal dimension as a function of size for 84 aggregates. Large aggregates possess fractal characteristics consistent with three-dimensional growth.

VI. CONCLUSION

We have studied colloid aggregation kinetics with a liquid-cell *in situ* TEM-STEM device, the nanoaquarium. We observed the motion and interactions of particles in liquid media in real time with nanoscale resolution, allowing us to gather information that cannot be obtained with any other technique. Our experiments provide a level of detail that previously could be afforded only by numerical simulations. To obtain similar information with frozen samples would be at best extremely tedious and at worst impossible. It should also be noted that the volume of solution needed in the experiment was very small ($<3\mu$L), making this an appealing technique when samples are scarce. The data collected with the nanoaquarium are consistent with prior observations obtained by other means [13–16], [32]. This is an important finding for establishing *in situ* liquid-cell TEM as an experimental technique that can produce meaningful results free from artifacts associated with the measurement technique. We also observed and explained an interesting growth regime in which large aggregates grown in a shallow nanochannel were found to possess fractal characteristics consistent with three-dimensional growth. Liquid-cell TEM with the nanoaquarium is likely to provide fundamental information in many scientific endeavors, such as self-assembly and controlled assembly of isotropic and anisotropic colloidal particles, electrochemical deposition, catalytic reaction, and interfacial phenomena.

ACKNOWLEDGMENTS

Device fabrication was carried out at the Cornell NanoScale Facility, a member of the National Nanotechnology Infrastructure Network, which is supported by the National Science Foundation (Grant No. ECS-0335765). Electron microscopy was performed at the Penn Regional Nanotechnology Facility. Frances M. Ross of IBM's T.J. Watson Research Center provided encouragement and advice. Sumant Sood of SUSS MicroTec shared expertise on wafer bonding. Peter Szczesniak of our machine shop assisted in constructing the device holder. This work was supported in part by the NSF-NIRT (CBET 0609062), NSF-NBIC (NSF NSEC DMR-0425780), and the Nanotechnology Institute of Ben Franklin Technology Partners of Southeastern Pennsylvania.

[1] J. M. Grogan and H. H. Bau, J. Microelectromech. Syst. **19**, 885 (2010).
[2] H. Zheng, S. A. Claridge, A. M. Minor, A. P. Alivisatos, and U. Dahmen, Nano Lett. **9**, 2460 (2009).
[3] M. J. Williamson, R. M. Tromp, P. M. Vereecken, R. Hull, and F. M. Ross, Nat. Mater. **2**, 532 (2003).
[4] A. Radisic, P. M. Vereecken, J. B. Hannon, P. C. Searson, and F. M. Ross, Nano Lett. **6**, 238 (2006).
[5] H. Zheng, R. K. Smith, Y.-wook Jun, C. Kisielowski, U. Dahmen, and A. P. Alivisatos, Science **324**, 1309 (2009).
[6] K.-L. Liu, C.-C. Wu, Y.-J. Huang, H.-L. Peng, H.-Y. Chang, P. Chang, L. Hsu, and T.-R. Yew, Lab Chip **8**, 1915 (2008).
[7] N. de Jonge, D. B. Peckys, G. J. Kremers, and D. W. Piston, Proc. Natl. Acad. Sci. U.S.A. **106**, 2159 (2009).
[8] D. B. Peckys, G. M. Veith, D. C. Joy, and N. de Jonge, PLoS ONE **4**, e8214 (2009).
[9] L. Mele, F. Santagata, G. Pandraud, B. Morana, F. D. Tichelaar, J. F. Creemer, and P. M. Sarro, J. Micromech. Microeng. **20**, 085040 (2010).
[10] J. F. Creemer, S. Helveg, G. H. Hoveling, S. Ullmann, A. M. Molenbroek, P. M. Sarro, and H. W. Zandbergen, Ultramicroscopy **108**, 993 (2008).
[11] E. A. Ring and N. de Jonge, Microsc. Microanal. **16**, 622 (2010).
[12] J. F. Creemer, S. Helveg, P. J. Kooyman, A. M. Molenbroek, H. W. Zandbergen, and P. M. Sarro, J. Microelectromech. Syst. **19**, 254 (2010).
[13] D. A. Weitz and M. Oliveria, Phys. Rev. Lett. **52**, 1433 (1984).
[14] D. A. Weitz, J. S. Huang, M. Y. Lin, and J. Sung, Phys. Rev. Lett. **54**, 1416 (1985).
[15] M. Y. Lin, H. M. Lindsay, D. A. Weitz, R. Klein, R. C. Ball, and P. Meakin, J. Phys. Condens. Matter **2**, 3093 (1990).
[16] M. Y. Lin, H. M. Lindsay, D. A. Weitz, R. C. Ball, R. Klein, and P. Meakin, Nature (London) **339**, 360 (1989).
[17] R. L. Penn, J. Phys. Chem. B **108**, 12707 (2004).
[18] F. Huang, H. Zhang, and J. F. Banfield, Nano Lett. **3**, 373 (2003).
[19] C. Ribeiro, E. J. H. Lee, E. Longo, and E. R. Leite, Chem. Phys. Chem. **6**, 690 (2005).
[20] F. Family, P. Meakin, and J. M. Deutch, Phys. Rev. Lett. **57**, 727 (1986).
[21] N. V. Brilliantov and P. L. Krapivsky, J. Phys. A **24**, 4789 (1991).
[22] V. Privman, D. V. Goia, J. Park, and E. Matijevic, J. Colloid Interface Sci. **213**, 36 (1999).
[23] J. Park, V. Privman, and E. Matijevic, J. Phys. Chem. B **105**, 11630 (2001).
[24] T. O. Drews, M. A. Katsoulakis, and M. Tsapatsis, J. Phys. Chem. B **109**, 23879 (2005).
[25] J. Zhang, F. Huang, and L. Zhang, Nanoscale **2**, 18 (2010).
[26] K.-S. Cho, D. V. Talapin, W. Gaschler, and C. B. Murray, J. Am. Chem. Soc. **127**, 7140 (2005).
[27] Y.-wook Jun, M. F. Casula, J.-H. Sim, S. Y. Kim, J. Cheon, and A. P. Alivisatos, J. Am. Chem. Soc. **125**, 15981 (2003).
[28] R. L. Penn and J. F. Banfield, Am. Mineral. **83**, 1077 (1998).
[29] R. L. Penn and J. F. Banfield, Science **281**, 969 (1998).
[30] C. Ribeiro, E. Longo, and E. R. Leite, Appl. Phys. Lett. **91**, 103105 (2007).
[31] See supplemental material at [http://link.aps.org/supplemental/10.1103/PhysRevE.83.061405] for video and further details on image processing.
[32] P. Meakin, Phys. Scr. **46**, 295 (1992).